

**Vortex-induced quantum metallicity in the mono-unit-layer superconductor NbSe<sub>2</sub>**Satoru Ichinokura,<sup>1,\*</sup> Yuki Nakata,<sup>2</sup> Katsuaki Sugawara,<sup>2,3</sup> Yukihiro Endo,<sup>1</sup> Akari Takayama,<sup>1</sup>  
Takashi Takahashi,<sup>2,3,4</sup> and Shuji Hasegawa<sup>1</sup><sup>1</sup>*Department of Physics, The University of Tokyo, 7-3-1 Hongo, Bunkyo-ku, Tokyo 113-0033, Japan*<sup>2</sup>*Department of Physics, Tohoku University, Sendai 980-8578, Japan*<sup>3</sup>*Center for Spintronics Research Network, Tohoku University, Sendai 980-8577, Japan*<sup>4</sup>*WPI Research Center, Advanced Institute for Materials Research, Tohoku University, Sendai 980-8577, Japan*

(Received 17 August 2018; published 5 June 2019)

We performed *in situ* magnetoresistance measurements in the ultrahigh-vacuum environment to reveal the quantum phase transitions of single unit-layer NbSe<sub>2</sub> epitaxially grown on bilayer graphene. It was found that the superconductor-normal state transition caused by the surface-normal magnetic field was intermediated by a quasimetallic state. This behavior is consistent with the “Bose metal” picture where a finite dissipation is caused by the breaking of phase coherence due to strong gauge-field fluctuation. On one hand, around the mean-field critical temperature, the onset of transition from the normal state to the low-temperature states was governed by the amplitude-fluctuation effect, prominently under the magnetic field. We applied scaling theories to determine the phase boundaries. The result of scaling analyses revealed a complex but essential phase diagram of the single unit-layer NbSe<sub>2</sub> as a two-dimensional superconductor.

DOI: [10.1103/PhysRevB.99.220501](https://doi.org/10.1103/PhysRevB.99.220501)**I. INTRODUCTION**

Since the theoretical proposal by Ginzburg in 1964 [1], two-dimensional superconductivity (2DSC) has attracted considerable interest because it involves a variety of fundamental issues, such as the fluctuation effect [2], dynamics of vortex [3], strong anisotropy of critical magnetic field [4], and the quantum phase transition (QPT) from the superconductor to insulator [5]. These two-dimensional phenomena have been observed in amorphous or granular films, which are thinner than the superconducting coherence length, since the 1980s [6]. Afterward, the development of nanoscale engineering made it possible to create thinner two-dimensional crystals, and finally reached the atomic scale thickness [7]. Now such 2DSCs are attracting renewed interest as subjects of not only fundamental physics but also material sciences because of their engineering capability based on band structures arising from the well-defined crystal structures. The molecular beam epitaxy (MBE) is a strong method to grow those crystalline 2DSC systems, for example, metallic overlayers on semiconductors [8–12] and ultrathin high-temperature superconductors on oxides [13]. On the other hand, superconductivity in free-standing 2D materials has been intensively explored and is realized in bilayer graphene with twisting [14] or metal intercalation [15].

Layered transition metal dichalcogenides have been known since the 1960s, as thermoelectric materials [16]. Recently, their transition from the bulk to the atomically thin limit has attracted much attention; e.g., the indirect-direct transition of band gap [17], the Zeeman-type spin splitting connected to the

valley degrees of freedom [18], and the high electron mobility [19]. Not only are these significant advantages for applications in electronic, optical, and spintronic devices but also exotic many-body phenomena such as the charge density wave (CDW) [20] and the superconductivity [21] are also widely studied as fundamental topics in low-dimensional materials. NbSe<sub>2</sub> is one of the intensively investigated superconductors since it also possesses a robust CDW [22,23] and a huge enhancement of the in-plane upper critical magnetic field of superconductivity due to the spin splitting in the electron pockets [24,25]. In addition to these anomalous phenomena related to spin-polarized electronic states, intriguing electromagnetic responses arising from the two-dimensional nature have been observed under the out-of-plane magnetic field; a quasimetallic state called “Bose metal (BM)” is induced by a very small magnetic field in exfoliated bilayer flakes [26]. This report created a lot of interest in revealing the ground state of a pure 2DSC in the presence of strong fluctuations, as investigated in 2DSCs formed in electrical-double-layer-transistors (EDLT) [27,28]. More recently, epitaxially grown single unit-layer (1UL) NbSe<sub>2</sub> was reported to exhibit the quantum Griffith singularity at QPT from superconductor to insulator in a high magnetic field, where the divergence of the dynamical critical exponent was observed [25]. However, a delicate change of resistance properties of superconducting 1UL NbSe<sub>2</sub> at the low-field region is still unclear because only *ex situ* transport measurements have been performed so far, with capping layers to protect very thin materials which, however, may perturb their smooth transition to the zero-resistance state.

In this work, we report the result of *in situ* magnetoelectrical transport measurements in ultrahigh-vacuum (UHV) to avoid oxidation/contamination on the surface and study the essential properties of superconducting 1UL NbSe<sub>2</sub>

\*Current address: Department of Physics, Tokyo Institute of Technology, Tokyo 152-8551, Japan; [ichinokura@phys.titech.ac.jp](mailto:ichinokura@phys.titech.ac.jp)

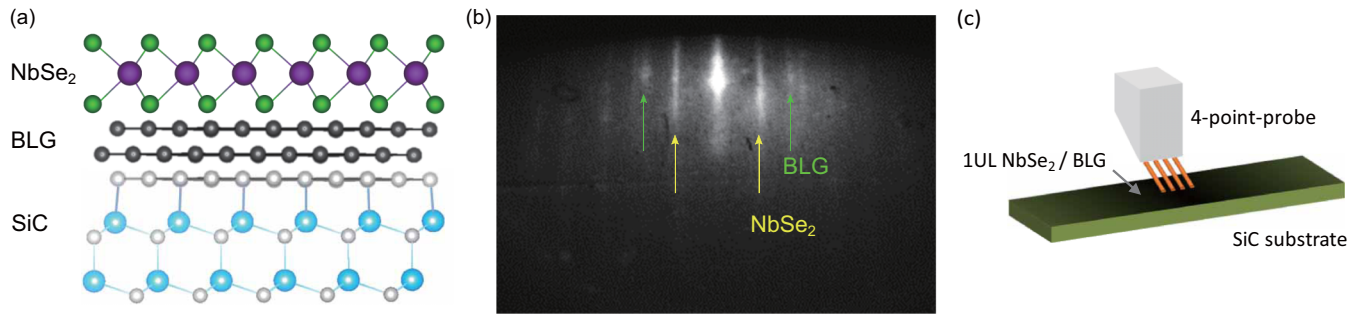


FIG. 1. (a) Schematic of a sectional view of the crystal structure of 1UL  $2H$ -NbSe<sub>2</sub>/bilayer graphene (BLG) on SiC substrate. Atoms colored by green, purple, black (gray), and blue represent Se, Nb, C, and Si, respectively. (b) RHEED pattern of the present sample. Streaks indicated by yellow arrows are diffraction spots from NbSe<sub>2</sub>, while those indicated by green arrows are from the underlying graphene. (c) Schematic of electrical transport measurements. Four-point probe directly touches on 1UL NbSe<sub>2</sub> in UHV.

epitaxially grown on bilayer graphene [Fig. 1(a)] with no capping layer. We found that a small magnetic field in the out-of-plane direction caused multiple phase transitions. Around the lowest temperature, an expected quantum-phase transition from the superconductor to the normal state is disrupted by an intervening “metallic” state. This phase is confirmed by a scaling theory [29,30], which describes the intermediation in interacting bosons picture. On the other hand, at around superconducting transition temperature  $T_c = 1.51$  K, the onset of transition from the normal state towards these ground states was governed by the amplitude-fluctuation effect. In the presence of the magnetic field, the amplitude fluctuation was treated by another scaling theory [31,32], which made it possible to interpolate a hidden phase boundary in the mean-field phase transition. We propose a detailed phase diagram of the mean-field region based on the multiple scaling methods.

## II. METHOD

A 1UL NbSe<sub>2</sub> film was grown on bilayer graphene by MBE [22,23]. First, an  $n$ -type Si-rich  $6H$ -SiC(0001) single-crystal wafer was heated at 1100 °C for 20 min in UHV of less than  $1.0 \times 10^{-9}$  Torr to form a bilayer graphene sheet on the surface of the crystal. The 1UL NbSe<sub>2</sub> film was grown by vapor deposition of Nb in Se atmosphere at  $5.0 \times 10^{-9}$  Torr on the bilayer-graphene substrate kept at 500 °C. The as-grown film was annealed at 400 °C for 30 min, resulting in the formation of atomically flat and uniform terraces. To perform the electrical transport measurements in a separate UHV chamber, the surface of NbSe<sub>2</sub> film was protected with a capping layer of amorphous Se to transfer it in the air. The capping layer was removed by annealing in the measurement chamber. The survival of NbSe<sub>2</sub> film was confirmed by reflection-high-energy electron diffraction (RHEED), which clearly showed sharp streaks derived from single crystalline NbSe<sub>2</sub> [Fig. 1(b)]. The electrical transport measurements were carried out with Unisoku USM-1300S, where a linear four-point-probe (4PP) consisting of four copper wires of 100  $\mu$ m in diameter with the probe spacing of approximately 200  $\mu$ m was attached to the probe stage. This 4PP directly contacts on the 1UL NbSe<sub>2</sub> in UHV as schematically drawn in Fig. 1(c). The sheet resistance  $R_{\text{sheet}}$  was obtained by the 4PP dc current-voltage measurements [33].

## III. RESULTS AND DISCUSSION

Figure 2(a) shows the sheet resistance  $R_{\text{sheet}}$  as a function of temperature under zero magnetic field  $B$ . Although the bulk NbSe<sub>2</sub> turns into a CDW state at 33 K [20], we did not observe any signature of CDW below 40 K. This is reasonable because the monolayer NbSe<sub>2</sub> shows the CDW transition at 145 K [34], much higher than that of bulk. At around 1.5 K, it shows a sharp drop from 680  $\Omega$ , suggesting the onset of superconductivity. The midpoint of the resistance drop represents the mean-field critical temperature of  $T_c = 1.51 \pm 0.01$  K, which is lower than that reported value by an *ex situ* transport measurement ( $T_c = 3.5$  K) [25], whereas the fact that no shoulder structure is observed suggests the uniformity of the present sample. The “zero” resistance appears below 1.4 K. The deviation between these two characteristic temperatures is due to the inevitable fluctuation arising from the two-dimensional nature, where the zero resistance is achieved by binding of a thermally generated vortex-antivortex pair (VP) at  $T_{\text{BKT}}$ , [called as Berezinskii-Kosterlitz-Thouless (BKT) transition] [2]. At a temperature range  $T_{\text{BKT}} < T < T_c$ , unbound vortices and antivortices cause a finite resistance  $R$  described by Halperin-Nelson theory [2]:  $R \propto \exp[-2b\{(T_c - T_{\text{BKT}})/(T - T_{\text{BKT}})\}^{1/2}]$ , where  $b$  is a material-dependent parameter. A successful fitting with this equation is displayed in Fig. 2(a) (inset), which estimates  $T_{\text{BKT}} = 1.387 \pm 0.004$  K.

Type-II 2DSC allows the magnetic field to penetrate in the out-of-plane direction. As shown in Fig. 2(b), the  $T_c$  value in 1UL NbSe<sub>2</sub> monotonically reduces upon increasing  $B$  and finally, the superconductivity disappears at  $B = 1.6$  T. Also, the  $R_{\text{sheet}}-T$  curves are obviously deformed by the magnetic field, while in the three-dimensional superconductors, the resistance curves rigidly shift to low temperatures. When the magnetic field is applied, the  $R_{\text{sheet}}-T$  curves start sluggishly to drop at the beginning of the transition from the normal state and have inflection points before reaching the minimum temperature limit as seen in the close-up scale displayed in the inset of Fig. 2(b). This complex behavior of resistivity suggests the presence of multiple-phase transitions with several boundaries in  $B$ - $T$  space. To more clearly see the quantum-phase boundaries, we show the upper critical fields  $B_{c2}(T_c)$  [open triangles in Fig. 2(c)] estimated from a conventional method, in which  $B_{c2}(T_c)$  is defined at half

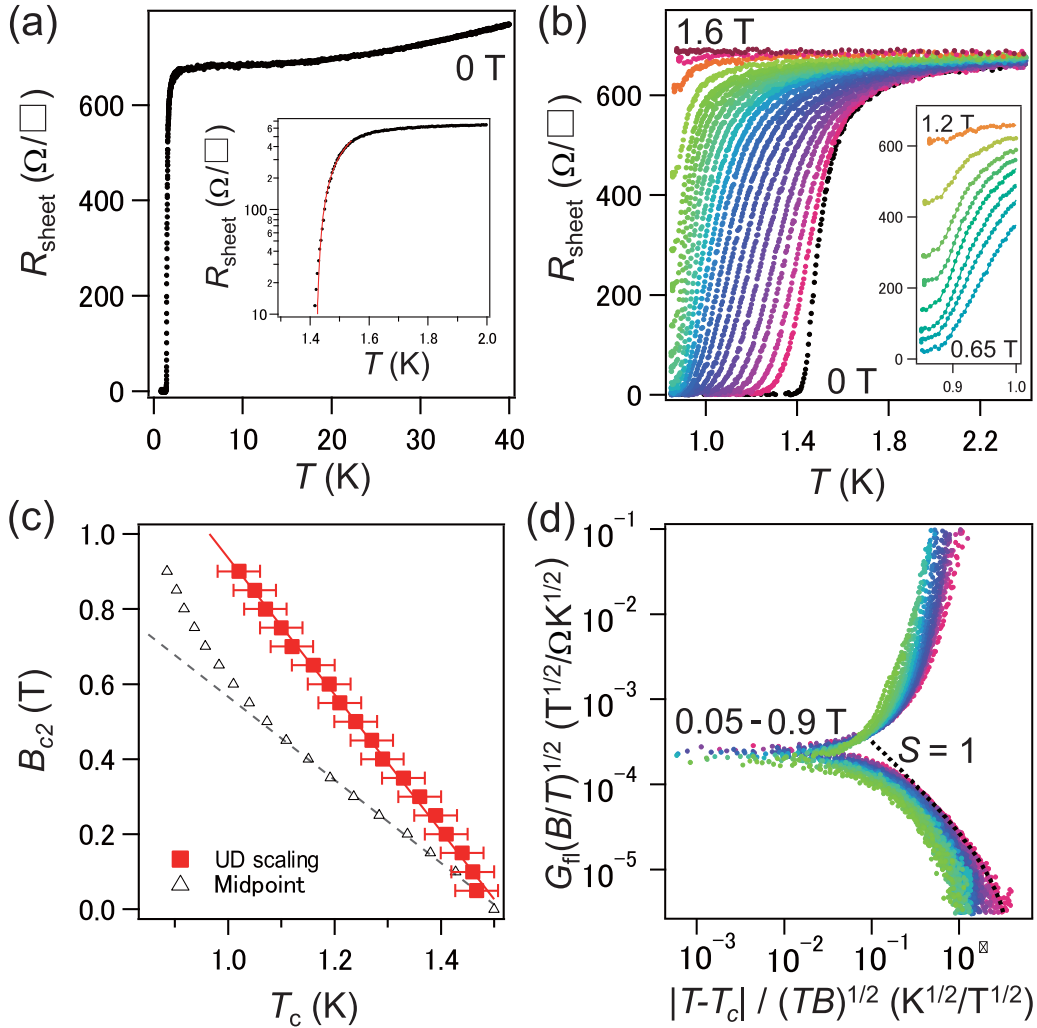


FIG. 2. Electrical transport properties of the 1UL 2H-NbSe<sub>2</sub>/bilayer graphene. (a) Temperature dependence of sheet resistivity under zero magnetic field. The abrupt change from zero to 680 Ω indicates the emergence of superconductivity at 1.51 K. Inset shows a closed-up resistivity curve from 1.3 to 2.0 K in semilogarithmic scale. The red solid line indicates the fitting result by Halperin-Nelson equation [2]. (b) Temperature dependence of sheet resistivity under a fixed magnetic field. It increases in step  $\Delta B = 0.05$  T from 0.0 to 0.9 T, and  $\Delta B = 0.2$  T from 1.0 to 1.6 T. Inset shows a closeup of  $R_{\text{sheet}}-T$  curves  $0.65 \leq B \leq 1.2$  T. (c) Comparison of the temperature-dependent upper critical field defined in two different ways. Black open triangles represent the midpoint of resistivity curves, which shows an upturn towards low temperature, apart from the linear region guided by the gray dashed line. Red filled squares represent interpolated  $(T_c, B_{c2})$  from UD scaling of fluctuation conductivity. (d) Result of UD scaling. The  $R_{\text{sheet}}(T)$  at  $0.05 \leq B \leq 0.9$  T is replotted with variable change. Here,  $T_c$  is appropriately chosen to reproduce the universal function in Eq. (1). The red solid line in (c) indicates numerical fitting with GL theory [4].

of the normal-state resistance as a function of temperature. This method is useful to obtain  $B_{c2}(T_c)$  at the vicinity of the zero-magnetic field since it shows the almost linear relation expected from the Ginzburg-Landau (GL) theory [a dashed line in Fig. 2(c)] [4]. However, the present result shows an unexpected upturn at a lower temperature ( $< 1.1$  K), suggesting that the mean-field critical point has a slight deviation from the midpoint due to the deformation of the resistivity curves. This is clearly different from the behavior of the upper critical field in the bulk NbSe<sub>2</sub>, which shows the convex upward expected by Werthamer-Helfand-Hohenberg theory [35]. In 2DSC, it is known that the excess conductance is generated by the fluctuation of the superconducting order parameter. Ullah and Dorsey (UD) calculated this effect by considering the fluctuation up to the second-order contributions to the free-energy expansion using a Hartree approximation, which

made it possible to precisely interpolate the mean-field critical point in the presence of magnetic field [31,32]. The excess conductivity  $G_{\text{fl}} \equiv 1/R_{\text{sheet}} - 1/R_N$  under different magnetic fields is scaled with the following universal relation [28,36]:

$$G_{\text{fl}} \left( \frac{B}{T} \right)^{1/2} = F_{\text{fl}} \left( \frac{T - T_c}{(TB)^{1/2}} \right), \quad F_{\text{fl}}(x) \propto \begin{cases} -x (x \ll 0) \\ x^{-s} (x \gg 0) \end{cases} \quad (1)$$

The parameter  $s$  is a parameter closely related to the dimensionality of the sample. For the two-dimensional case  $s = 1$  is predicted [36]. The variable  $T_c$  in Eq. (1) is a mean-field superconducting transition temperature in the presence of a magnetic field, and is used as a fitting parameter of the scaling. The function  $F_{\text{fl}}(x)$  is an arbitrary function proportional to  $x$  at  $x \ll 0$  limit (low temperature), while it approaches  $x^{-s}$  at  $x \gg 0$  limit (high temperature) as described in Eq. (1). This theory

TABLE I. Comparison of the basic superconducting parameters in NbSe<sub>2</sub> with various thicknesses.

Thickness	Growth method	$T_c$ [K]	$B_{c2}(0)$ [T]	$\xi_{GL}$ [nm]	$U(0)/k_B$ [K]
1UL <sup>a</sup>	MBE	$1.51 \pm 0.01$	$2.76 \pm 0.03$	$10.94 \pm 0.06$	$10.3 \pm 0.5$
1UL <sup>b</sup>	MBE	3.5	2.16	12.3	NA
1UL <sup>c</sup>	Exfoliation	3.0	2.6	11	NA
2UL <sup>d</sup>	Exfoliation	5.26	2.7	8.9	27.5
2nm <sup>e</sup>	MBE	3.725	2.6	10.4	1800
Bulk <sup>f</sup>	Single crystal	7.0	5.1	7.4	NA
Bulk <sup>g</sup>	Single crystal	7.3	5.3	8.5	NA

<sup>a</sup>This work; <sup>b</sup>Reference [25]; <sup>c</sup>Reference [24]; <sup>d</sup>Reference [26]; <sup>e</sup>Reference [3]; <sup>f</sup>Reference [35]; <sup>g</sup>Reference [37]

suggests that the data sets for different temperatures and fields should scale  $G_{fl}(B/T)^{1/2} = (1/R_{sheet} - 1/R_N)(B/T)^{1/2}$  plotted versus  $(T - T_c)/(TB)^{1/2}$  by tuning  $T_c$  for each data set. Actually, the variable transformation of  $R_{sheet}(T)$  results in the universal relation as plotted in Fig. 2(d) by tuning  $T_c$  as a fitting parameter under each magnetic field. The lower branch is approximately equal to a relation in  $x^{-1}$  as indicated by the black dashed line in Fig. 2(d), consistent with the theoretically expected  $F_{fl}(x)$  form as in other examples of 2DSCs [28,31,32,36]. The validity of the scaling is confirmed by plotting the newly interpolated  $B_{c2}$ - $T_c$  relation from the scaling as in Fig. 2(c) (red filled squares), which obeys a linear relation expected from the GL theory [4]. The coherence length  $\xi_{GL}$  was estimated as  $10.94 \pm 0.06$  nm by the fitting. In Table I, we compare the coherence length among the present and previous studies on NbSe<sub>2</sub> with various thicknesses. The  $\xi_{GL}$  distributes around  $9.9 \pm 2.5$  nm.

At the middle of resistance dropping,  $R_{sheet}$ - $T$  curves under the magnetic field in Fig. 2(b) still have finite gradients depending on  $B$ . This feature is known to be caused by the thermally activated flux flow (TAFF) in the vortex state [3]. The resistance  $R$  generated by dissipation due to TAFF is described by  $R \propto \exp(-U(B)/k_B T)$ , where  $U(B)$  is the activation energy. Figure 3(a) depicts the Arrhenius plot of  $R_{sheet}$  as a function of  $1/T$  at fixed magnetic fields in the semi-log scale. At weak fields less than 0.30 T, one can see the linear relation that is consistent with the TAFF behavior,

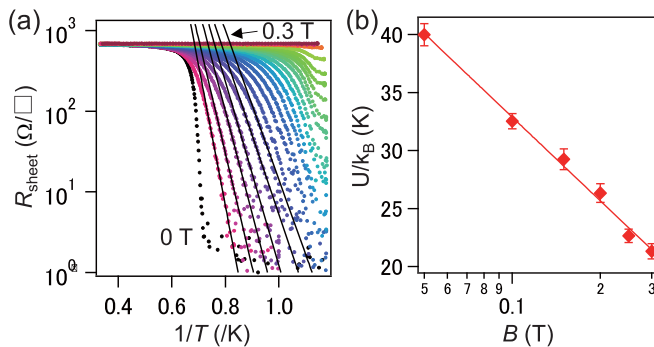


FIG. 3. (a) Arrhenius plot of resistivity, which is converted from data in Fig. 2(b) with the same color code. The black solid lines indicate the fitting by  $R \propto \exp(-U(B)/k_B T)$ , where  $U(B)$  is an activation energy. (b) The activation energy extrapolated from the fitting in (a), plotted as a function of the magnetic field  $B$ . The red solid line is the least-squares fitting by  $U(B) = U_0 \ln(B^*/B)$ .

as confirmed by fittings indicated by black solid lines. At a field stronger than 0.30 T, the TAFF behavior is hidden by the gradual dropping of resistivity, possibly due to the strong effect of amplitude-fluctuation discussed above. The extrapolated  $U(B)$  at the weak field is plotted as a function of the magnetic field in Fig. 3(b), which indicates a relation  $U(B) = U_0 \ln(B^*/B)$ . This is in accordance with the TAFF model in a 2D vortex lattice system [36]. The numerical fitting gives  $B^* = 2.4 \pm 0.3$  T and  $U(0)/k_B = 10.3 \pm 0.5$  K. According to the model [36],  $B^*$  is a melting field of the vortex lattice, which approximately equals  $B_{c2}(0)$ . The critical magnetic field at 0 K is extrapolated by the linear fitting in Fig. 2(c) as  $B_{c2}(0) = 2.76 \pm 0.03$  T, showing a reasonable agreement with  $B^*$ . As clearly seen in Table I,  $U(0)/k_B$ , which indicates the strength of pinning of vortices, is much smaller in both 1UL (this work) and 2UL (Ref. [26]) samples than in a 2-nm-thick sample (Ref. [3]). This weak pinning is thought to contribute to the Bose metallic state observed in the 1–2UL samples as discussed below.

Here, we discuss the QPTs at low temperature. The most classical example of the QPT is the superconductor-insulator (SI) transition, induced by disorder or magnetic field. This is thought as a transition between two ground states of a Cooper pair (CP): from a condensed state as a superconductor to a localized one as an insulator. However, it is clear that the present data does not agree with the direct SI transition because the  $R_{sheet}$ - $T$  curves saturate toward the lowest temperature with finite residual resistivities as seen in Fig. 2(b) (inset) under a magnetic field larger than 0.6 T. Recently, this intermediating “metallic” state is observed in highly crystalized 2DSCs [26–28], which attracts considerable attention as a different ground state. Several models are proposed as the origin of the finite residual resistance, e.g., quantum creep motion of vortices [27,28] and dissipation caused by loss of global phase coherence in CPs [26]. The latter is called “phase glass” or the BM state. This is a quantum phase intervening between the insulating (INS) and superconducting state (SC), which is theoretically proposed [29,30,38,39]. In this picture, as an analogue of the BKT transition, unbinding of VP destroys the phase coherence of the CP and causes a resistive transition. In the case of a magnetic-field-induced transition, first, the dynamic gauge-field fluctuation drives unbinding of the VPs, which breaks the resistance-free SC state. However, the CP system does not necessarily turn into the INS state immediately; The INS state of CPs is realized when unbound vortices and antivortices condense into a superfluid (SF) state as a bosonic system. This is driven by the zero-point motion of

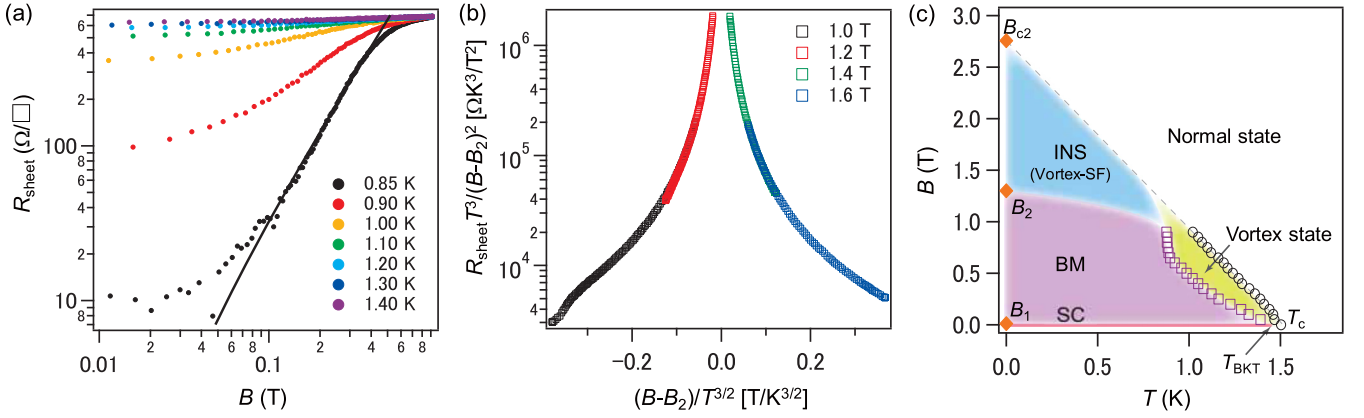


FIG. 4. (a), (b) Application of scaling theories at transitions from (a) SC–BM, and (b) BM–INS phases [29,30,38,39]. In (a), sheet resistivity  $R_{\text{sheet}}$  at fixed temperatures was measured as a function of the magnetic field.  $R_{\text{sheet}}(B)$  at 0.85 K showing a power-law dependence described by Eq. (2). The fitting result in Eq. (2) is shown as a black solid line. (b) Another variable transformation of  $R_{\text{sheet}}(T, B)$  function reproducing the universal curve in Eq. (3) at  $1.0 \leq B \leq 1.6$  T. (c) Schematically drawn phase diagram of superconductivity-related states in 1UL NbSe<sub>2</sub>. Black open circles are the same points as red squares in Fig. 2(d), which represent the mean-field transition point. Gray dashed line is the result of the GL fitting. Purple open squares are inflection points between the TAFF-like behavior and saturation of resistivity. Orange filled diamonds show the critical field of QPTs at absolute zero temperature extrapolated from the scaling behavior of Eqs. (1)–(3). The true SC region (indicated by the red bar) lies near the  $B = 0$  axis. Phase boundaries are drawn to smoothly connect the experimental data points.

(anti)vortices. However, in the moderately disordered 2DSC, it is interfered by the gauge field fluctuation under a finite but sufficiently small magnetic field, which converts the vortices-antivortices system into a non-SF liquid state. Due to the duality, when the vortex system is liquid, the Cooper pair system is also liquid, viz. the BM state. The BM is broken into the INS state when the further magnetic field increases the zero-point motion until it overcomes the gauge field fluctuation. Therefore, the two-step phase transition (i) from SC to BM and (ii) from BM to INS is expected to be induced by a magnetic field. Each transition shows an independent scaling behavior for resistivity, which determines the phase boundaries at the low temperature.

First, we discuss the (i) *SC-BM transition*. The film enters a metallic state when VPs are unbound due to the gauge field fluctuations [29,30,38,39]. Resistivity, induced by the free dislocations, across the transition from SC to BM is described by a simple formula of magnetoresistance [30]

$$R \propto (B - B_1)^{2\nu_1}. \quad (2)$$

Here,  $B_1$  and  $\nu_1$  are the critical field and the exponent of this step of the phase transition, respectively. Figure 4(a) displays the  $R_{\text{sheet}}-B$  plot of 1UL NbSe<sub>2</sub> on the log-log scale. The curve at 0.85 K obeys a power-law dependence with respect to the magnetic field, which is well reproduced by Eq. (2). The solid black line in Fig. 4(a) shows the successful fitting results obtained at  $B_1 = 0.011 \pm 0.007$  T and  $\nu_1 = 0.88 \pm 0.03$ . Here,  $B_1$  shows a very small, but reasonable value because the energy barriers from stable (SC) to metastable (BM) states are nonzero but so small in a disordered 2D system that even the zero-point motion and dynamical gauge field fluctuations would destabilize the SC phase.

Next (ii) the *BM-INS transition* is discussed. As the magnetic field is increased further beyond another critical value  $B_2$ , the quantum zero-point motion of vortices increases and overtakes the gauge field fluctuation. Since it is regarded as a second-order phase transition, Das and Doniach proposed

a two-parametric scaling formula extended from the single-parametric one of the SC-INS transition by phenomenological consideration as follows [30]:

$$\frac{RT^{1+2/z_2}}{(B - B_2)^{\nu_2(z_2+2)}} = F_{\text{BI}}\left(\frac{B - B_2}{T^{1/\nu_2 z_2}}\right), \quad (3)$$

where  $F_{\text{BI}}$  is some universal function including  $B_2$  and  $(z_2, \nu_2)$ , the critical field and the exponents of this step of the phase transition, respectively. We applied this two-parametric scaling to the present 1UL NbSe<sub>2</sub>. Figure 4(b) indicates that  $R_{\text{sheet}}-T$  curves within  $1.0 \leq B \leq 1.6$  T are clearly replotted into two branches, i.e., the BM side (left branch,  $B = 1.0$  and 1.2 T) and the insulator side (right branch,  $B = 1.4$  and 1.6 T) as expected in Ref. [30], when  $B_2 = 1.3$  T is assumed.

We have estimated the critical magnetic field  $B_1$ ,  $B_2$ , and  $B_{c2}$  at the respective quantum phase boundaries in 1UL NbSe<sub>2</sub>, which are summarized in Fig. 4(c) as a schematic quantum-phase diagram. First, it is divided into the normal state and the others by the mean-field phase boundary indicated by the gray dashed line, which is extrapolated from the black open circles, the same as temperature-dependent upper critical fields in Fig. 2(c). Notice that the present system gradually transits from the normal state at temperatures higher than the boundary due to amplitude fluctuation of the superconducting order parameter, as described by the UD scaling theory. At zero magnetic field, the NbSe<sub>2</sub> turns into a resistance free, i.e., SC through the mechanism of the BKT transition at  $T_{\text{BKT}}$ . When a small magnetic field up to  $B_1$  ( $\sim 0.01$  T) is applied, finite resistance appears. The origin of this saturation to residual resistance is interpreted as the BM state according to the two scaling approaches that determine the phase boundaries at  $B_1$  and  $B_2$  ( $\sim 1.3$  T) [indicated by orange filled diamonds at 0 K in Fig. 4(c)]. When the BM phase is warmed up across the inflection indicated by purple open squares, it turns into the classical vortex-penetrated state, which has dissipation caused by TAFF. Above 1.3 T, the BM state is broken by superfluidity of vortex and the NbSe<sub>2</sub>

film turns into an INS state. However, it exists up to  $B_{c2}$ , until the magnetic flux penetrates the entire region of the two-dimensional superconductor.

It has been pointed out that the quantum metallic state smoothly connects to the Griffith's singularity state in EDLT-ZrNCl and MoS<sub>2</sub> [28]. Even though the suggested mechanisms of quantum metal are different from each other, it is a natural analogy that the BM state transits into the quantum Griffith state in 1UL NbSe<sub>2</sub> above  $B_2$ . The present study complements the phase diagram between the true superconducting and the Griffith state. Future work will solve the relationship between the vortex-superfluid state and the quantum Griffith's singularity by measuring a precise  $R$ - $B$  relationship at various temperatures with a fine temperature step at the vicinity of superconductor-normal metal transition.

#### IV. CONCLUSION

In conclusion, by *in situ* electrical transport measurements of single unit layer NbSe<sub>2</sub> in UHV, an anomalous quasimetallic state, which mediates the transition from the superconductor to the insulator, was found to be generated by a small out-of-plane magnetic field. The scaling analysis based on the model of the Bose metal explained well the two-step transition, suggesting the existence of a bosonic ground

state. We also found that the phase boundary of mean-field superconductivity was determined by the scaling theory by Ullah and Dorsey, meaning that the amplitude fluctuation dominates the onset of superconductivity. Our results strongly support the theoretical consideration of universality in the two-dimensional superconductors, where the fluctuations in both phase and amplitude play the most important role in the magnetoelectric response.

#### ACKNOWLEDGMENTS

We thank R. Akiyama and R. Hobara at The University of Tokyo, and T. Sato at Tohoku University for their useful discussions. This work was supported by the JSPS (KAKENHI JP15J11055, JP25246025, JP15H02105, JP18H01821, JP18H01160, JP18J10038) and the MEXT (Grant-in-Aid for Scientific Research on Innovative Areas "Science of Atomic Layers" JP25107003 and "Molecular Architectonics" JP25110010), and the Program for Key Interdisciplinary Research. Also acknowledged is a grant for Basic Science Research Projects from the Sumitomo Foundation, Science Research Projects from Iketani Science and Technology Foundation, the Program for Key Interdisciplinary Research, and World Premier International Research Center, Advanced Institute for Materials Research.

- 
- [1] V. L. Ginzburg, *Phys. Lett.* **13**, 101 (1964).
- [2] B. I. Halperin and D. R. Nelson, *J. Low Temp. Phys.* **36**, 599 (1979).
- [3] J. W. P. Hsu and A. Kapitulnik, *Phys. Rev. B* **45**, 4819 (1992).
- [4] M. Tinkham, *Introduction to Superconductivity* (Courier Corporation, North Chelmsford, MA, 1996).
- [5] D. B. Haviland, Y. Liu, and A. M. Goldman, *Phys. Rev. Lett.* **62**, 2180 (1989).
- [6] A. M. Goldman, *Low Temp. Phys.* **36**, 884 (2010).
- [7] T. Uchihashi, *Supercond. Sci. Technol.* **30**, 013002 (2017).
- [8] T. Uchihashi, P. Mishra, M. Aono, and T. Nakayama, *Phys. Rev. Lett.* **107**, 207001 (2011).
- [9] M. Yamada, T. Hirahara, and S. Hasegawa, *Phys. Rev. Lett.* **110**, 237001 (2013).
- [10] Y. Xing H. -M. Zhang, H. -L. Fu, H. Liu, Y. Sun, J. -P. Peng, F. Wang, X. Lin, X. -C. Ma, Q. -K. Xue, J. Wang, and X. C. Xie, *Science* **350**, 542 (2015).
- [11] A. V. Matetskiy, S. Ichinokura, L. V. Bondarenko, A. Y. Tupchaya, D. V. Gruznev, A. V. Zotov, A. A. Saranin, R. Hobara, A. Takayama, and S. Hasegawa, *Phys. Rev. Lett.* **115**, 147003 (2015).
- [12] S. Ichinokura, L. V. Bondarenko, A. Y. Tupchaya, D. V. Gruznev, A. V. Zotov, A. A. Saranin, and S. Hasegawa, *2D Mater.* **4**, 025020 (2017).
- [13] J. F. Ge, Z. L. Liu, C. Liu, C. L. Gao, D. Qian, Q. K. Xue, Y. Liu, and J. F. Jia, *Nat. Mater.* **14**, 285 (2015).
- [14] Y. Cao, V. Fatemi, S. Fang, K. Watanabe, T. Taniguchi, E. Kaxiras, and P. Jarillo-Herrero, *Nature (London)* **556**, 43 (2018).
- [15] S. Ichinokura, K. Sugawara, A. Takayama, T. Takahashi, and S. Hasegawa, *ACS Nano* **10**, 2761 (2016).
- [16] X. Zhou, D. Yang, and R. F. Frindt, *J. Phys. Chem. Solids* **57**, 1137 (1996).
- [17] Y. Zhang, T. R. Chang, B. Zhou, Y. T. Cui, H. Yan, Z. Liu, F. Schmitt, J. Lee, R. Moore, Y. Chen, H. Lin, H. T. Jeng, S. K. Mo, Z. Hussain, A. Bansil, and Z. X. Shen, *Nat. Nanotechnol.* **9**, 111 (2014).
- [18] K. Sugawara, T. Sato, Y. Tanaka, S. Souma, and T. Takahashi, *Appl. Phys. Lett.* **107**, 071601 (2015).
- [19] X. Cui, G. H. Lee, Y. D. Kim, G. Arefe, P. Y. Huang, C. H. Lee, D. A. Chenet, X. Zhang, L. Wang, F. Ye, F. Pizzocchero, B. S. Jessen, K. Watanabe, T. Taniguchi, D. A. Muller, T. Low, P. Kim, and J. Hone, *Nat. Nanotechnol.* **10**, 534 (2015).
- [20] K. Sugawara, Y. Nakata, R. Shimizu, P. Han, T. Hitosugi, T. Sato, and T. Takahashi, *ACS Nano* **10**, 1341 (2016).
- [21] E. Morosan, H. W. Zandbergen, B. S. Dennis, J. W. G. Bos, Y. Onose, T. Klimczuk, A. P. Ramirez, N. P. Ong, and R. J. Cava, *Nat. Phys.* **2**, 544 (2006).
- [22] Y. Nakata, K. Sugawara, S. Ichinokura, Y. Okada, T. Hitosugi, T. Koretsune, K. Ueno, S. Hasegawa, T. Takahashi, and T. Sato, *npj 2D Mater. Appl.* **2**, 12 (2018).
- [23] M. M. Ugeda, A. J. Bradley, Y. Zhang, S. Onishi, Y. Chen, W. Ruan, C. Ojeda-Aristizabal, H. Ryu, M. T. Edmonds, H.-Z. Tsai, A. Riss, S.-K. Mo, D. Lee, A. Zettl, Z. Hussain, Z.-X. Shen, and M. F. Crommie, *Nat. Phys.* **12**, 92 (2015).
- [24] X. Xi, Z. Wang, W. Zhao, J.-H. Park, K. T. Law, H. Berger, L. Forró, J. Shan, and K. F. Mak, *Nat. Phys.* **12**, 139 (2015).
- [25] Y. Xing, K. Zhao, P. Shan, F. Zheng, Y. Zhang, H. Fu, Y. Liu, M. Tian, C. Xi, H. Liu, J. Feng, X. Lin, S. Ji, X. Chen, Q. K. Xue, and J. Wang, *Nano Lett.* **17**, 6802 (2017).

- [26] A. W. Tsen, B. Hunt, Y. D. Kim, Z. J. Yuan, S. Jia, R. J. Cava, J. Hone, P. Kim, C. R. Dean, and A. N. Pasupathy, *Nat. Phys.* **12**, 208 (2015).
- [27] Y. Saito, Y. Kasahara, J. Ye, Y. Iwasa, and T. Nojima, *Science* **350**, 409 (2015).
- [28] Y. Saito, T. Nojima, and Y. Iwasa, *Nat. Commun.* **9**, 778 (2018).
- [29] D. Das and S. Doniach, *Phys. Rev. B* **60**, 1261 (1999).
- [30] D. Das and S. Doniach, *Phys. Rev. B* **64**, 134511 (2001).
- [31] S. Ullah and A. T. Dorsey, *Phys. Rev. Lett.* **65**, 2066 (1990).
- [32] S. Ullah and A. T. Dorsey, *Phys. Rev. B* **44**, 262 (1991).
- [33] M. Yamada, T. Hirahara, R. Hobara, S. Hasegawa, H. Mizuno, Y. Miyatake, and T. Nagamura, *e-J. Surf. Sci. Nanotechnol.* **10**, 400 (2012).
- [34] X. Xi, L. Zhao, Z. Wang, H. Berger, L. Forro, J. Shan, and K. F. Mak, *Nat. Nanotechnol.* **10**, 765 (2015).
- [35] A. Nader and P. Monceau, *SpringerPlus* **3**, 16 (2014).
- [36] M. H. Theunissen and P. H. Kes, *Phys. Rev. B* **55**, 15183 (1997).
- [37] N. Toyota, H. Nakatsuji, K. Noto, A. Hoshi, N. Kobayashi, Y. Muto, and Y. Onodera, *J. Low Temp. Phys.* **25**, 485 (1976).
- [38] P. Phillips and D. Dalidovich, *Science* **302**, 243 (2003).
- [39] D. Dalidovich and P. Phillips, *Phys. Rev. Lett.* **89**, 027001 (2002).